J. Plasma Fusion Res. SERIES, Vol. 8 (2009)

Theory and Simulations of Parallel Electric Fields in Nonlinear Magnetosonic Waves: Three-Component Plasma

Seiichi TAKAHASHI and Yukiharu OHSAWA

Department of Physics, Nagoya University, Nagoya 464-8602, Japan

(Received: 29 August 2008 / Accepted: 4 November 2008)

The parallel electric field $E_\parallel$ and its integral along the magnetic field F $(= -\int E_\parallel ds)$ in nonlinear magnetosonic waves are studied with theory and fully kinetic, electromagnetic, particle simulations. The magnitudes of $E_\parallel$ and F in small-amplitude pulses are analytically obtained for warm plasmas and for cold plasmas. Furthermore, it is found that the simulation values of F in large-amplitude waves (shock waves) are explained by a simple phenomenological relation. The parallel electric field becomes weak and nonstationary as the positron density increases. This is also studied with simulations.

Keywords: electron-positron-ion plasma, parallel electric field, nonlinear magnetosonic wave, shock wave, nonstationarity, particle simulation

1. Introduction

It has been demonstrated with relativistic electromagnetic, particle simulations that positrons can be accelerated to ultrarelativistic energies $\gamma \sim 2000$ by an oblique magnetosonic shock wave in an electron-positron-ion (e-p-i) plasma [1–3]. In this acceleration mechanism, the time rate of change of γ is proportional to the electric field $E_\parallel$ parallel to the magnetic field [1, 2]. It is thus important to find the magnitude of $E_\parallel$ to quantitatively understand this acceleration mechanism. In addition, it was shown with particle simulations that the positron acceleration is weak when the positron density n_{p0} is high [1,2]. This may also be explained if we know the dependence of $E_\parallel$ on n_{p0}.

Recently, a theory was developed on $E_\parallel$ in nonlinear magnetosonic waves in an electron-ion plasma, and its predictions were verified with simulations [4]. In this paper, we extend this work to e-p-i plasmas. Furthermore, we investigate the nonstationarity of $E_\parallel$ with simulations.

In Sec. 2, we analyze small-but-finite amplitude, magnetosonic waves with the three-fluid model to find that the integral of $E_\parallel$ along the magnetic field, $F = -\int E_\parallel ds$, which we call the parallel pseudo potential, is proportional to the difference of electron and positron pressures, $p_{e0} - p_{p0}$, in a warm plasma while it is proportional to the magnetic pressure in a cold plasma [5]. Moreover, the theory indicates that F decreases with an increasing n_{p0}.

In Sec. 3, we investigate the nonstationarity of the parallel electric field in large-amplitude magnetosonic shock waves by means of one-dimensional electromagnetic, particle simulations. The simulations show that the parallel pseudo potential F becomes dependent on time more strongly as n_{p0} increases.

In Sec. 4, we summarize our work. These results that F becomes smaller and more time-dependent with increasing n_{p0} explain the previous simulation result that the acceleration is weak when n_{p0} is high.

2. Dependence of Parallel Electric Field on Positron Density

We analytically obtain $E_\parallel$ and F in small-but-finite amplitude ($\epsilon < 1$) nonlinear magnetosonic waves propagating in the x direction in an external magnetic field $\boldsymbol{B}_0 = B_0(\cos\theta, 0, \sin\theta)$ in a three-component plasma. Applying the reductive perturbation method [6] to the three-fluid model with finite temperatures, we obtain the Korteweg-de Vries (KdV) equation [5]. In this perturbation scheme, the lowest-order, parallel electric field $E_\parallel$ and parallel pseudo potential F are given [5] as

$$eE_{\parallel\mathrm{T}} = -\epsilon^{3/2}\frac{\omega_{pe}^2}{\omega_p^2 n_{e0}}\left(\Gamma_e p_{e0} - \Gamma_p p_{p0} - \frac{m_e}{m_i}\frac{\Gamma_i p_{i0}}{Z}\right)\sin\theta\cos\theta\frac{\partial}{\partial\xi}\left(\frac{B_{z1}}{B_0}\right), \quad (1)$$

$$eF_{\mathrm{T}} = \epsilon\frac{\omega_{pe}^2}{\omega_p^2 n_{e0}}\left(\Gamma_e p_{e0} - \Gamma_p p_{p0} - \frac{m_e}{m_i}\frac{\Gamma_i p_{i0}}{Z}\right)\sin\theta\frac{B_{z1}}{B_0}, \quad (2)$$

where the subscripts e, p, and i refer to the electrons, positrons, and ions, respectively, Γ_j ($j = e, p$, or i) denotes the specific heat ratio, n_{j0} is the equilibrium density, p_{j0} is the equilibrium thermal pressure, m_j is the mass, Z is the ionic charge state (the ion charge is $q_i = Ze$ with e the elementary electric charge), ξ is the

author's e-mail: takahashi.seiichi@a.mbox.nagoya-u.ac.jp

stretched coordinate corresponding to the space coordinate x [5,6], B_{z1} is the perturbed magnetic field in the z-direction, ω_{pj} is the plasma frequency, and ω_p^2 is defined as $\omega_p^2 = \sum_j \omega_{pj}^2$. We have used the subscript T to indicate that $E_\parallel$ and F are determined by temperatures. If we ignore the ion terms with $\sim O(m_e/m_i)$ in Eqs. (1) and (2), the parallel electric field $E_{\parallel \mathrm{T}}$ and parallel pseudo potential F_{T} are proportional to the difference of electron and positron pressures, $p_{e0} - p_{p0}$. Both $E_{\parallel \mathrm{T}}$ and F_{T} become small when n_{p0}/n_{e0} is high.

In the cold plasma limit ($T_j = 0$), the parallel electric field (1) and parallel pseudo potential (2) both vanish. In this limit, we carry out higher order calculations to obtain [5]

$$E_{\parallel \mathrm{B}} = \epsilon^{5/2} \frac{4\pi \tilde{v}_{\mathrm{A}}^4}{B_0^2 \tan\theta} \left(\sum_j \frac{n_{j0} m_j^2}{q_j} \right) \times \left(\frac{c}{\omega_p} \right)^2 \frac{\partial^3}{\partial \xi^3} \left(\frac{B_{z1}}{B_0} \right), \quad (3)$$

$$F_{\mathrm{B}} = -\epsilon^2 \frac{4\pi \tilde{v}_{\mathrm{A}}^4}{B_0^2 \sin\theta} \left(\sum_j \frac{n_{j0} m_j^2}{q_j} \right) \times \left(\frac{c}{\omega_p} \right)^2 \frac{\partial^2}{\partial \xi^2} \left(\frac{B_{z1}}{B_0} \right), \quad (4)$$

where q_j is the electric charge, $-q_e = q_p = q_i/Z = e$, and $\tilde{v}_{\mathrm{A}}$ is defined with use of the light speed c and the Alfvén speed v_{A} as

$$\tilde{v}_{\mathrm{A}}^2 = \frac{v_{\mathrm{A}}^2}{1 + v_{\mathrm{A}}^2/c^2}. \quad (5)$$

In this cold plasma limit, $E_\parallel$ and F are proportional to the magnetic pressure, $B_0^2/8\pi$ (if $v_{\mathrm{A}}^2 \ll c^2$). Thus, the subscript B is used for $E_\parallel$ and F in Eqs. (3) and (4).

The dispersion relation of the magnetosonic wave can be written as $\omega/k = v_{\mathrm{mp0}}(1 + \mu k^2)$, where v_{mp0} is the phase velocity in the long-wavelength limit and μ is the dispersion coefficient. As shown in the top panel of Fig. 1, the critical angle θ_c, at which μ becomes zero, decreases with increasing n_{p0}/n_{e0}. It indicates that if the propagation angle is $\theta = 89°$, $\theta > \theta_c$ and μ does not become zero at any value of n_{p0}/n_{e0}. If $\theta = 85°$, however, μ becomes zero at $n_{p0}/n_{e0} \simeq 0.8$.

As shown in the middle panel of Fig. 1, if $\theta = 89°$, the magnitude of F_{B} in a solitary wave decreases with increasing n_{p0}/n_{e0}. If $\theta = 85°$, F_{B} diverges at $n_{p0}/n_{e0} \simeq 0.8$ at which $\mu = 0$. Except for the vicinity of the point of $\mu = 0$, F_{B} decreases with n_{p0}/n_{e0}.

The above theory is for small-amplitude pulses. Concerning the large-amplitude [$\epsilon \sim O(1)$] waves (shock waves), it has been found that the following

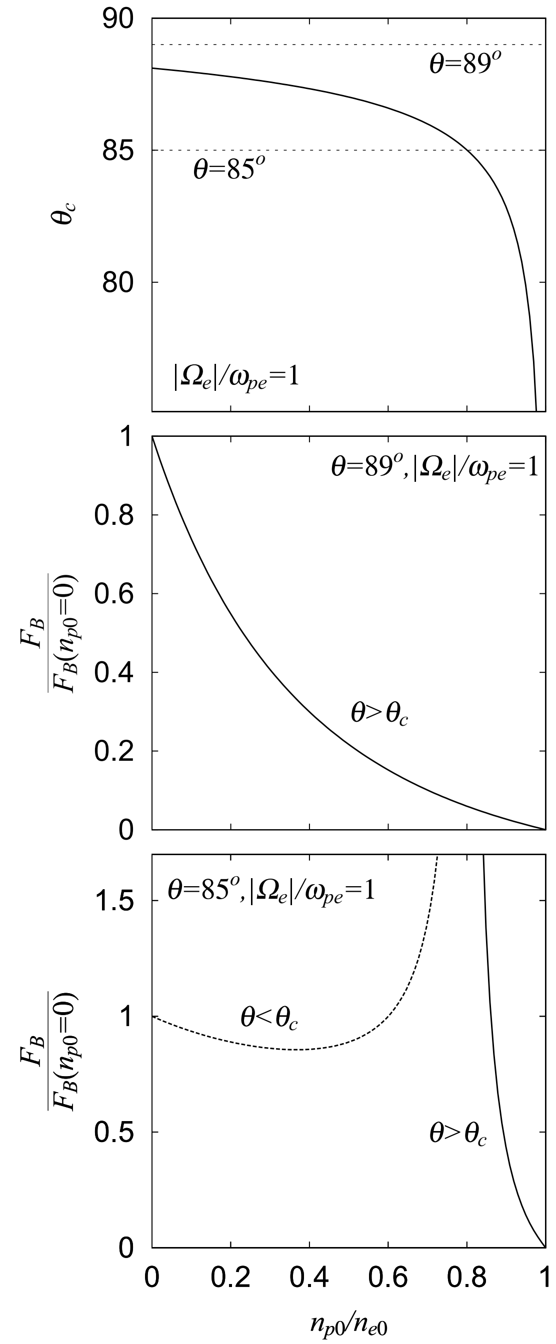

Fig. 1 Critical angle θ_c (top panel) and peak values of F_{B} of solitary waves (middle and bottom panels) as functions of n_{p0}/n_{e0}. The middle and bottom panels show the cases of $\theta = 89°$ and of $\theta = 85°$, respectively. Here, we have assumed that the ratio of the electron gyrofrequency to plasma frequency is $|\Omega_e|/\omega_{pe} = 1$.

phenomenological expression for F,

$$eF \sim \left(\frac{B_0^2}{4\pi n_{e0}} + \Gamma_e T_e \right) \left(1 - \frac{n_{p0}}{n_{e0}} \right) \frac{B_{z1}}{B_0}, \quad (6)$$

fits to the observed values of F in shock simulations in both warm and cold plasmas [5]. The magnitude of F given by Eq. (6) also becomes small as n_{p0} increases.

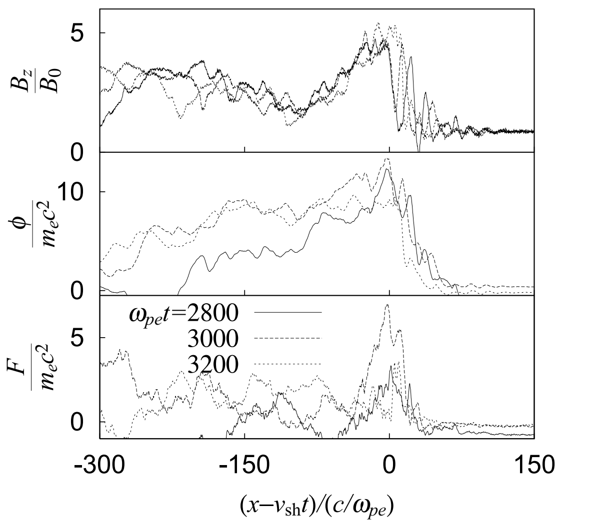

Fig. 2 Profiles of B_z, ϕ, and F in a shock wave. The profile of F rapidly varies with time.

3. Nonstationarity of Parallel Electric Field

3.1 Simulation model and parameters

As n_{p0}/n_{e0} rises, the nonstationarity of F is enhanced, as well as the magnitude of F decreases. In this section, we investigate the nonstationarity of F with one-dimensional (one space coordinate and three velocities), relativistic, electromagnetic particle simulations with full particle dynamics, by observing magnetosonic shock waves propagating in the x direction in an external magnetic field $\boldsymbol{B}_0 = B_0(\cos\theta, 0, \sin\theta)$. For the method of particle simulations of shock waves, see Refs. [7–9].

The simulation parameters are as follows: The total system length is $L = 16384\Delta_g$, where Δ_g is the grid spacing; the number of electrons is 6.1×10^5; the ion-to-electron mass ratio is $m_i/m_e = 400$ with $m_p = m_e$; the propagation angle is $\theta = 60°$; and the ratio of electron gyrofrequency to plasma frequency is $|\Omega_e|/\omega_{pe} = 1.0$. The light speed is $c/(\omega_{pe}\Delta_g) = 10$. The temperatures are the same, $T_e = T_p = T_i$, and the thermal velocities are $v_{Te}/(\omega_{pe}\Delta_g) = v_{Tp}/(\omega_{pe}\Delta_g) = 0.26$ and $v_{Ti}/(\omega_{pe}\Delta_g) = 0.013$.

3.2 Simulation result

Figure 2 shows the profiles of B_z, electric potential ϕ, and F at three different times of a shock wave. The profile of F depends on time more strongly than those of B_z and ϕ do. To study the nonstationarity of F more quantitatively, we examine the time variation of $F_{\max}(t)$, where $F_{\max}(t)$ is the maximum value of $F(x, t)$ at a time t. Figure 3 shows $F_{\max}(t)$, which is normalized to its time average $\langle F_{\max}(t)\rangle$, for low and high n_{p0} cases; i.e., for $n_{p0}/n_{e0} = 0.1$ and $n_{p0}/n_{e0} = 0.6$. The amplitude of $F_{\max}(t)/\langle F_{\max}(t)\rangle$ is much larger in the high n_{p0} case than in the low n_{p0} case.

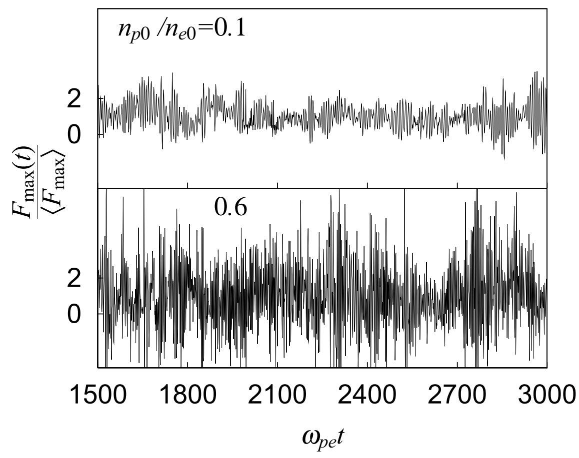

Fig. 3 Time variations of $F_{\max}(t)/\langle F_{\max}\rangle$.

Figure 4 shows the spectra of $F_{\max}(t)$ (upper panel) and $\phi_{\max}(t)$ (lower panel) for $n_{p0}/n_{e0} = 0.1$ and 0.6. The Fourier amplitudes $\hat{F}_{\max}(\omega)$ for $n_{p0}/n_{e0} = 0.6$ are greater than those for $n_{p0}/n_{e0} = 0.1$ for most of the frequencies. It is interesting to note that there is a hump near $\omega/\omega_{pe} = 1$ (ω_{pe} is the plasma frequency of the electrons in the upstream region) for $n_{p0}/n_{e0} = 0.1$ and this hump is enhanced in the region $1 \lesssim \omega/\omega_{pe} \lesssim 3$ for $n_{p0}/n_{e0} = 0.6$. The amplitude $\hat{\phi}_{\max}(\omega)$ is small and does not change much for $\omega/\omega_{pe} \gtrsim 0.1$. For $\omega/\omega_{pe} \lesssim 0.1$, it is slightly enhanced in the high n_{p0} case.

In Fig. 5 we plot the relative standard deviations of $F_{\max}(t)$ and $\phi_{\max}(t)$,

$$\langle(\delta F_{\max})^2\rangle = \frac{\langle[\langle F_{\max}(t)\rangle - F_{\max}(t)]^2\rangle^{1/2}}{\langle F_{\max}\rangle}, \quad (7)$$

$$\langle(\delta \phi_{\max})^2\rangle = \frac{\langle[\langle \phi_{\max}(t)\rangle - \phi_{\max}(t)]^2\rangle^{1/2}}{\langle \phi_{\max}\rangle}, \quad (8)$$

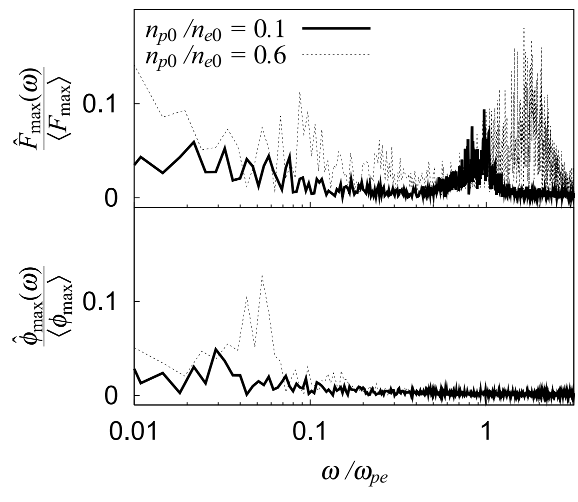

Fig. 4 Fourier amplitudes of $F_{\max}(t)$ and $\phi_{\max}(t)$.

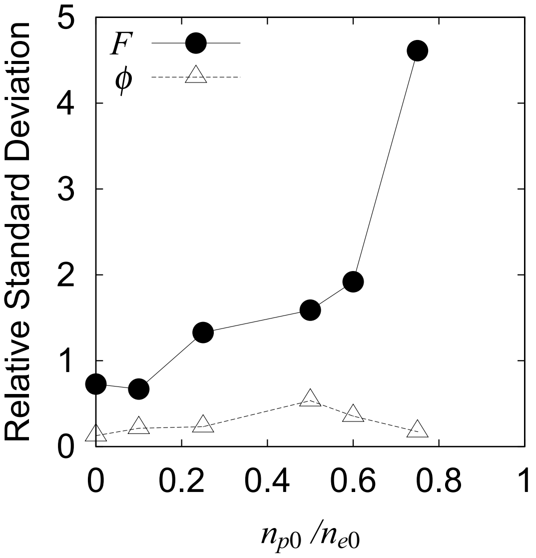

Fig. 5 Relative standard deviations of $F_{\max}(t)$ and $\phi_{\max}(t)$.

as functions of the positron density n_{p0}/n_{e0}. The closed circles and open triangles, respectively, represent $\langle(\delta F_{\max})^2\rangle$ and $\langle(\delta\phi_{\max})^2\rangle$. The dependence of the relative standard deviation of ϕ on the positron density is rather weak, while that of F significantly rises as n_{p0}/n_{e0} increases, indicating that the nonstationarity of F is enhanced when n_{p0}/n_{e0} is large.

Figure 6 shows the contour maps of $|E_{\parallel}(k,\omega)|$ and of $|E_x(k,\omega)|$ for the shock wave when $n_{p0}/n_{e0} = 0.1$. We find that the values of $|E_{\parallel}(k,\omega)|$ and $|E_x(k,\omega)|$ are large near the dispersion curve of the magnetosonic wave. In addition, $|E_{\parallel}(k,\omega)|$ is fairly large in the high-frequency regime $1 \lesssim \omega/\omega_{pe} \lesssim 3$ in the long-wavelength region $ck/\omega_{pe} \lesssim 2$. We do not find large $|E_x(k,\omega)|$, however, in the high frequency regime. This is consistent with Fig. 4, where $\hat{\phi}_{\max}(\omega)$ is small for $\omega/\omega_{pe} \gtrsim 1$ while $\hat{F}_{\max}(\omega)$ has a peak near $\omega/\omega_{pe} = 1$. We then see that the transverse electric fields in the high-frequency waves with $\omega \gtrsim \omega_{pe}$ [10] affect the nonstationarity of F. Figure 4 indicates that their effect is more significant where n_{p0}/n_{e0} is large.

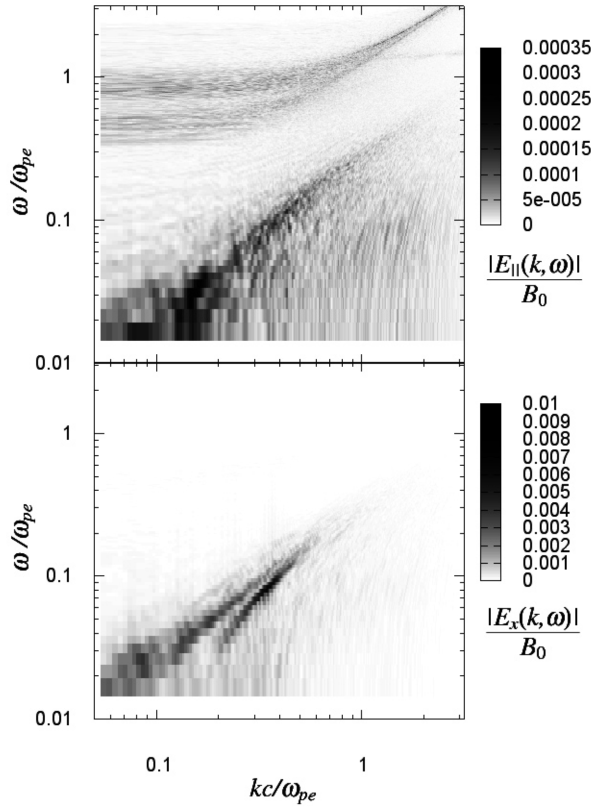

Fig. 6 Contour maps of $|E_{\parallel}(k,\omega)|$ and $|E_x(k,\omega)|$ in shock wave.

4. Summary

We have studied the parallel electric field in nonlinear magnetosonic waves in e-p-i plasmas with theory and particle simulations. The theory based on the three-fluid model indicates that the parallel pseudo potential F $(= -\int E_{\parallel} ds)$ in small-amplitude waves with $\epsilon < 1$ is proportional to the difference of electron and positron pressures, $p_{e0} - p_{p0}$, in warm plasmas and to magnetic pressure, $B_0^2/8\pi$, in cold plasmas. Furthermore, the theory shows that F becomes small with increasing positron density n_{p0} except for the vicinity of the point at which the dispersion coefficient μ becomes zero; F becomes zero at $n_{p0}/n_{e0} = 1$. Simulations show that as n_{p0}/n_{e0} rises, the nonstationarity of F is enhanced, as well as the magnitude of F decreases. These results are consistent with the simulation result [1, 2] that the positron acceleration becomes weak as n_{p0} increases. The simulation values of F in large-amplitude waves (shock waves) are explained by a phenomenological relation (6) for both warm and cold plasmas.

[1] H. Hasegawa, S. Usami and Y. Ohsawa, Phys. Plasmas **10**, 3455 (2003).
[2] H. Hasegawa and Y. Ohsawa, Phys. Plasmas **12**, 012312 (2005).
[3] H. Hasegawa, K. Kato and Y. Ohsawa, Phys. Plasmas **12**, 082306 (2005).
[4] S. Takahashi and Y. Ohsawa, Phys. Plasmas **14**, 112305 (2007).
[5] S. Takahashi, M. Sato and Y. Ohsawa, Phys. Plasmas **15**, 082309 (2008).
[6] T. Kakutani, H. Ono, T. Taniuti and C.C. Wei, J. Phys. Soc. Jpn **24**, 1159 (1968).
[7] N. Bessho and Y. Ohsawa, Phys. Plasmas **6**, 3076 (1999).
[8] Y. Ohsawa, Phys. Fluids **28**, 2130 (1985).
[9] P.C. Liewer, A.T. Lin, J.M. Dawson and M.Z. Caponi, Phys. Fluids **24**, 1364 (1981).
[10] T.E. Stringer, J. Nuclear Energy Part C, **5**, 89 (1963).